Photoacoustic monitoring of burn healing process in rats

Kazuya Aizawa
Keio University
Department of Electronics and Electrical Engineering
3-14-1, Hiyoshi, Kohoku-ku
Yokohama, Kanagawa 223-8522, Japan
and
Japan Self Defense Force Central Hospital
1–2–24, Ikejiri, Setagaya-ku
Tokyo 154–8532, Japan

Shunichi Sato
National Defense Medical College Research Institute
Division of Biomedical Information Sciences
3-2, Namiki, Tokorozawa
Saitama 359-8513, Japan

Daizoh Saitoh
National Defense Medical College Research Institute
Division of Basic Traumatology
3-2, Namiki, Tokorozawa
Saitama 359-8513, Japan

Hiroshi Ashida
National Defense Medical College Research Institute
Division of Biomedical Information Sciences
3-2, Namiki, Tokorozawa
Saitama 359-8513, Japan

Minoru Obara
Keio University
Department of Electronics and Electrical Engineering
3-14-1, Hiyoshi, Kohoku-ku
Yokohama, Kanagawa 223-8522, Japan

Abstract. We performed multiwavelength photoacoustic (PA) measurement for extensive deep dermal burns in rats to monitor the healing process of the wounds. The PA signal peak at 532 nm, an isosbestic point for oxyhemoglobin (HbO_2) and deoxyhemoglobin (HHb), was found to shift to a shallower region of the injured skin tissue with the elapse of time. The results of histological analysis showed that the shift of the PA signal reflected angiogenesis in the wounds. Until 24 h postburn, PA signal amplitude generally increased at all wavelengths. We speculate that this increase in amplitude is associated with dilation of blood vessels within healthy tissue under the injured tissue layer and increased hematocrit value due to development of edema. From 24 to 48 h postburn, the PA signal showed wavelength-dependent behaviors; signal amplitudes at 532, 556, and 576 nm continued to increase, while amplitude at 600 nm, an HHb absorption-dominant wavelength, decreased. This seems to reflect change from shock phase to hyperdynamic state in the rat; in the hyperdynamic state, cardiac output and oxygen consumption increased considerably. These findings show that multiwavelength PA measurement would be useful for monitoring recovery of perfusion and change in local hemodynamics in the healing process of burns.
 [DOI: 10.1117/1.3028005]

Keywords: multiwavelength photoacoustic measurement; severe burn; healing process; angiogenesis; hemodynamics.

Paper 07498RR received Dec. 26, 2007; revised manuscript received Jul. 23, 2008; accepted for publication Sep. 5, 2008; published online Nov. 26, 2008. This paper is a revision of a paper presented at the SPIE conference on Photons Plus Ultrasound: Imaging and Sensing 2008: The Ninth Conference on Biomedical Thermoacoustics, Optoacoustics, and Acousto-Optics, February 2008, San Jose, California. The paper presented there appears (unrefereed) in SPIE Proceedings Vol. 6856.

1 Introduction

Because severe burns affect not only local injured tissue but also the whole body, both the local treatment for early wound closure and systemic management are required. For systemic management, treatment of shock in the early stage and treatment of multiple organ dysfunction syndrome in the late stage are crucial, and continuous, real-time monitoring of hemodynamics, including peripheral circulation, is required; severe burn patients show phase-dependent unique abnormalities in their circulation dynamics, which often cause inadequate delivery of oxygen to peripheral organs.[1,2] The plan for local treatment of burns critically depends on the depth, size, and location of the wounds. In terms of wound depth, burns can be classified into epidermal burns (EBs), superficial dermal burns (SDBs), deep dermal burns (DDBs), and deep burns or full-thickness burns.[3,4] EBs and SDBs can heal spontaneously in a relatively short term, while healing of DDBs is delayed, often resulting in scar formation. In most cases of full-thickness burns, necrotomy and skin grafting are needed because spontaneous reepithelialization does not occur. It should be noted that wound depth may be increased by infection, and careful attention should therefore be paid to the states of wounds.

The healing process of burns has three phases: inflammatory phase, proliferative phase, and remodeling phase.[5] After the inflammatory phase, structural changes in injured tissues, including angiogenesis, granulation tissue formation, and reepithelialization, occur and these changes can provide important information for assessing wound healing process.

In clinical practice, visual observation of the wound size, color, and eschar and a pin-prick test are widely used for burn diagnosis,[6,7] but this cannot provide quantitative information of injuries. For noninvasive burn diagnosis, various modalities, such as laser Doppler imaging (LDI),[8] thermography,[9] fluorescence imaging,[10] and polarization-sensitive optical coherence tomography (OCT),[11,12] have been investigated. LDI can capture the recovery of blood flow within the wounds, which is one of the important indicators of healing. Because recovered perfusion leads to the increased temperature of the

Address all correspondence to Shunichi Sato, Division of Biomedical Information Sciences, National Defense Medical College Research Institute, 3-2 Namiki, Tokorozawa, Saitama 359-8513, Japan. Tel: +81 4 2995 1384; Fax: +81 4 2991 1757; E-mail: shunsaot@ndmc.ac.jp.

1083-3668/2008/13(6)/064020/7/$25.00 © 2008 SPIE

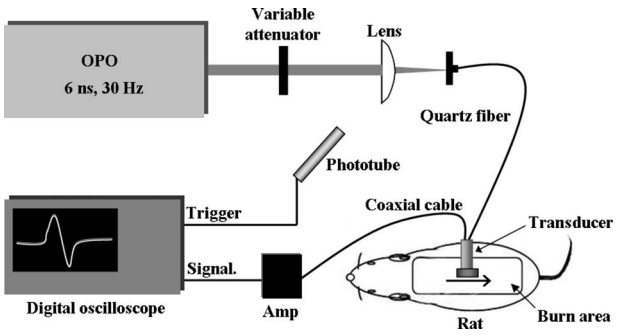

Fig. 1 Experimental setup for measurement of PA signals for rat burn models.

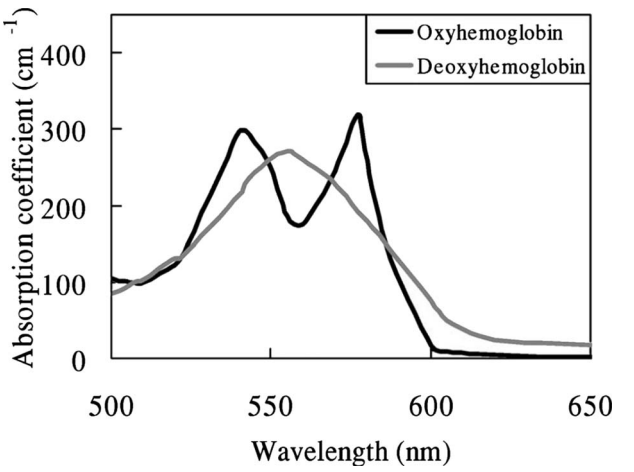

Fig. 2 Absorption spectra of oxyhemoglobin and deoxyhemoglobin in rats.[21]

wound surface, thermography can also provide information on wound healing. Fluorescence imaging is a technique to assess the increased permeability of injured blood vessels in burnt tissue by observing fluorescence originating from leaked indocyanine green that has been injected intravenously. However, these methods cannot provide quantitative depth information on depth of injuries. Epithelialization and granulation tissue formation associated with wound healing can be observed by polarization-sensitive OCT with a high spatial resolution, but measurable depth is limited to 1–2 mm, which is insufficient for clinical application.

In our previous study, we showed the validity of photoacoustic (PA) diagnosis of burns in rats *in vivo* at an early postburn time, a technique in which PA waves originating from the blood in healthy tissue under the injured tissue layer were measured on the wound surface with an axial resolution of ~100 μm and a lateral resolution of ~2 mm.[13,14] Propagation time of the PA waves gives information on the depth of blood perfusion and hence the depth of injuries. Recently, Zhang et al. reported application of PA microscopy to diagnosis of burns in a pig ex vivo, achieving much higher spatial resolutions: 15 μm in axial and 45 μm in lateral directions.[15] Advantages of our conventional PA measurement over PA microscopy for burn diagnosis may include lower sensitivity to motion artifacts, with sacrificing resolutions.

As described above, the severity of burns depends both on depth and area of injuries. When clinical application is considered, an axial resolution of ~100 μm enables differentiation between SDB and DDB and differentiation between DDB and full-thickness burn, because the thickness of typical human skin is much greater than this resolution, ranging from 1 to 3 mm. This axial resolution is also useful for planning debridement. For the size of burns, a rough estimation is valid; in practice, a doctor's palm is often used for area estimation for extended burns, and a lateral resolution of ~2 mm is therefore acceptable for determining clinically relevant burn severity.

The advantages of PA diagnosis of burns include the ease with which quantitative depth information can be obtained and greater sampling depth compared to those of OCT-based techniques. In addition, multiwavelength PA measurement can provide information on hemodynamics, such as blood oxygen saturation (SO_2) and total hemoglobin concentration,[16–18] which is important for systemic management of severe burns.[19]

In this study, we applied PA measurement to monitor the healing process of burns. We intended to detect the time-dependent recovery of blood perfusion in the wounds and also examined the change in the peripheral hemodynamics on the basis of multiwavelength measurement. We made DDBs in dorsal skins in rats and performed two-dimensional PA measurements for up to 120 h after injury. Depth profiles of the signals were compared to the results of histological analysis, and the wavelegth-dependent change in PA signals was analyzed.

2 Materials and Methods

2.1 *Burn Models*

Protocols in this study were approved by the Committee on Ethics of Animal Experiments in the National Defense Medical College. Male Wistar rats weighing 250–280 g were anesthetized with intraperitoneal injection of pentobarbital sodium (50 mg/kg animal weight), and dorsal hair was shaved and depilated with hair-removal cream. As a severe burn model, DDB of ~20% total body surface area was made by immersing rat dorsal skin in water at a temperature of 78 °C for 10 s with a Walker–Mason template.[20] Immediately after making the burn, saline solution (50 mL/kg animal weight) was intraperitoneally injected for resuscitation. We chose a rat model because the conditions for making a DDB are well established and there is a database of PA burn diagnosis using this model. The wounds were covered with nonadhering dressing (ADAPTIC, Johnson and Johnson), and the dressing was replaced every day. Between the measurements, rats were singly caged with free access to food and water at an ambient temperature in the range of 25–28 °C.

2.2 *Measurement of PA Signals*

The experimental setup for PA measurement is shown in Fig. 1. An optical parametric oscillator (OPO; MOPO-710, Spectral-Physics Lasers, CA; pulse width, 5 ns; repetition rate, 30 Hz) pumped by the third harmonics of an Nd:YAG laser (GCR290, Spectra-Physics Lasers, CA) was used as a light source for PA excitation; the output pulses were coupled to a quartz fiber with a core diameter of 600 μm. Pulse en-

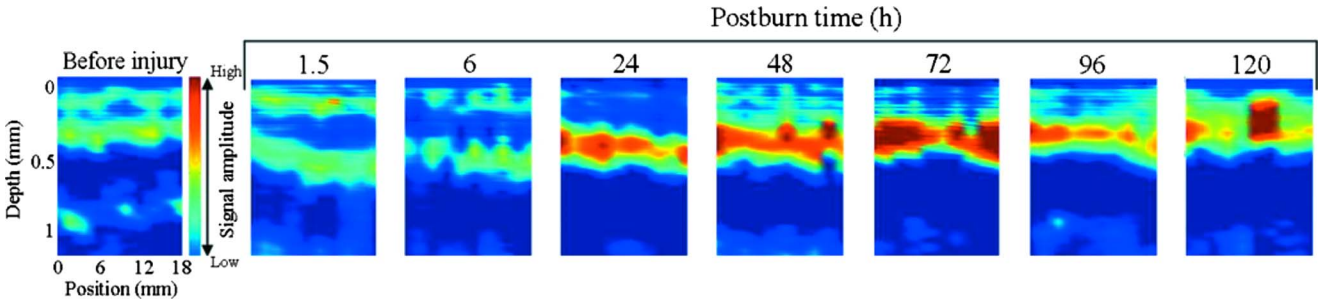

Fig. 3 Photoacoustic tomograms obtained by 532 nm, 6 ns pulsed light irradiation before and after making a deep dermal burn in rat skin. The horizontal axis and vertical axis indicate horizontal position and depth of the skin, respectively. The region of highest PA signal level is shown in red. (Color online only.)

ergy for irradiation was adjusted to 200 ± 10 μJ with a variable attenuator at all the wavelengths stated below. A ring-shaped P(VDF/TrFE) [poly(vinylidene fluoride-trifluoroethylene)] film (inner diameter, 3.5 mm; outer diameter, 5.5 mm; thickness, 30 μm) was used to detect PA signals. The angular detection aperture was ~20 deg. In the detector, the film and the output end of the fiber were coaxially arranged. Piezoelectric signals were amplified with an field-effect transistor amplifier and recorded in a digital oscilloscope (TDS3054B, Tektronics). Figure 2 shows the absorption spectra for oxyhemoglobin (HbO_2) and deoxyhemograbin (HHb) in rats.[21] We used four light wavelengths in this study: 532, 556, 576, and 600 nm. At 532 nm, HbO_2 and deoxyhemograbin HHb have the same molar extinction coefficients. Absorption of HbO_2 is much higher than that of HHb at 576 nm, while absorption of HHb is dominant at 556 and 600 nm; at 600 nm, absorption of HHb is about five-times larger than that of HbO_2.[21] PA signals were measured at postburn times of 1.5, 6, 12, 24, 48, 72, 96, and 120 h. At each point of measurement on the wound, PA measurement was repeated twice; in each measurement, signals induced by 64 light pulses were averaged, the total number of irradiated light pulses being 128 at each point. A PA detector was linearly scanned on the wound surface over a range of 18 mm at a 2-mm interval. PA signals obtained at each point were converted to depth profiles using an assumed sound velocity of 1500 m/s, and the depth profiles of PA signals were transformed into a tomogram by using MATLAB (6.5, Mathworks), where spline interpolation was used. It takes ~1 min to obtain one image. The depth profiles and amplitudes of PA signals obtained at each wavelength were compared.

2.3 *Histological Examination*

To investigate the validity of PA measurement, we performed histological analyses based on hematoxylin-eosin (HE) staining and immunohistochemical (IHC) staining with antirat CD31/PECAM-1 antibodies for assessing angiogenesis in the burned tissues, and we compared their results to PA signals. Specimens for the histological examinations were excised from rat dorsal skins after PA measurement at postburn times of 6, 48, and 120 h, and they were fixed in ethanol and embedded in paraffin blocks. After specimens had been sliced and stained, they were observed with a light microscope (Axiovert 200, ZEISS), and images were captured with a digital camera (Axiocam HRc, ZEISS). The numbers of pixels indicating CD31-positive were counted on the images, and their depth profiles were obtained; the profiles were compared to the depth profiles of PA signals.

2.4 *Statistical Analysis*

The depths of PA signal peaks giving the highest amplitudes were recorded. The data were statistically analyzed on the basis of the nonparametric Mann–Whitney test. A value of $P < 0.05$ was considered statistically significant. Changes in the amplitudes of PA signals obtained at an each wavelength from 1.5 to 120 h were analyzed on the basis of two-way analysis of variance with the two factors wavelength and time.

3 Results

3.1 *Time Courses of PA Signal at* 532 nm

Figure 3 shows PA tomograms obtained at a wavelength of 532 nm before and 1.5–120 h after making a deep dermal burn in rats. Although PA signals varied depending on the point of measurement, signal layers with low to high amplitude were observed in specific depth ranges; these signal layers are thought to originate from blood in the tissue. Before injury, three signal layers with low to medium amplitudes

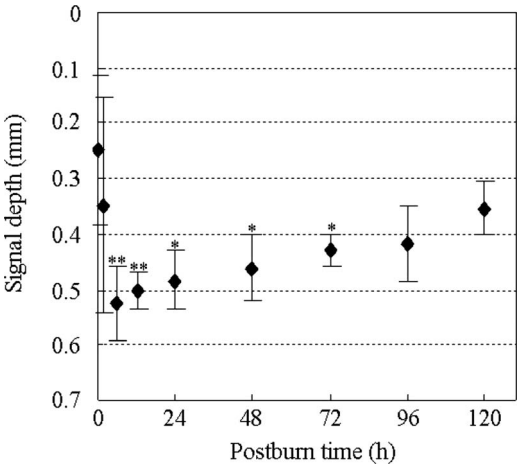

Fig. 4 Time course of signal peak depths at 532 nm (10 sites for each rat, $n=5-8$). Values are expressed as means±standard error ($^{*}P<0.01$, $^{**}P<0.001$, 120 h postburn time versus other postburn times).

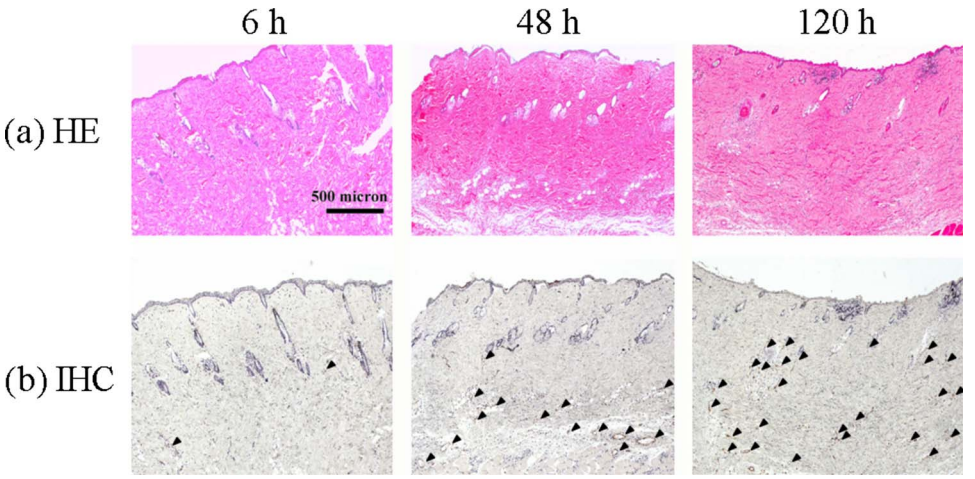

Fig. 5 Histologies of rat skin at 6, 48, and 120 h postburn times: (a) HE staining and (b) IHC staining with rat CD31 antibobies. Arrowheads indicate neovascularities.

were observed in the depth ranges of 0.1–0.2, 0.3–0.4, and 0.7–0.8 mm, while at the postburn time of 1.5 h, two signal layers with medium amplitudes were observed in the depth ranges of 0.1–0.2 and 0.4–0.6 mm. The first signal layer had almost disappeared at 6 h, indicating the occlusion of blood flow due to the injury, and the signal amplitude of the second layer became higher with the elapse of time. The second signal layer gradually shifted to a shallower region; the depth range of this layer was 0.3–0.4 mm at 120 h.

Figure 4 shows the time course of signal peak depth giving the highest amplitude at 532 nm. At 1.5 h, signal peak depth largely varied in the range of 0.15–0.55 mm, while the variation became smaller at 6 h, at which time signal peak depth ranged from 0.45 to 0.6 mm. The signal peak depth shifted to a shallower region with the elapse of time, indicating a decreased zone of stasis and hence the recovery of blood perfusion. Significant differences were observed between the signal peak depths at 6–12 h and that at 120 h ($P<0.001$) and between signal peak depths at 24–72 h and that at 120 h ($P<0.01$).

3.2 *Histological Analysis*

Figures 5(a) and 5(b) shows cross-sectional images of rat skins with H&E and IHC staining using antirat CD31 antibody, respectively, at postburn times of 6, 48, and 120 h. At 6 h, there was a small number of CD31-positive cells, indicating limited neovascularities, while at 48 h, a certain amount of neovascularities was observed in the middle and lower layers of the dermis. At 120 h, the density of neovascularities was increased drastically in a wide depth range of the dermis. Figure 6 shows the depth profiles of averaged CD31-positive pixel numbers at each postburn time ($n=4$). The distribution of neovascularities in the wounded tissues was extended with the elapse of time; high-density neovascularities were observed at ~1.2 mm at 6 h, at 0.7–1.2 mm at 48 h and at 0.2–1.2 mm at 120 h.

3.3 *Time Courses of PA Signal Amplitudes*

Figure 7 shows PA tomograms obtained at three other wavelengths of 556, 576, and 600 nm before and 6–120 h after

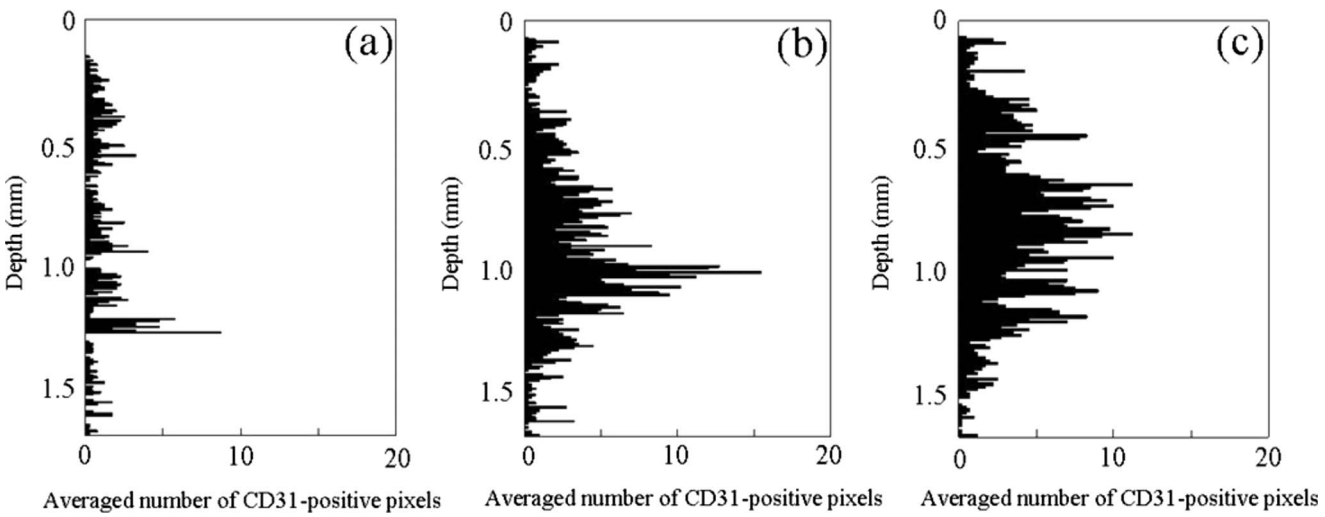

Fig. 6 Depth profiles of pixels indicating CD31-positive at (a) 6, (b) 48, and (c) 120 h after making the burn ($n=4$).

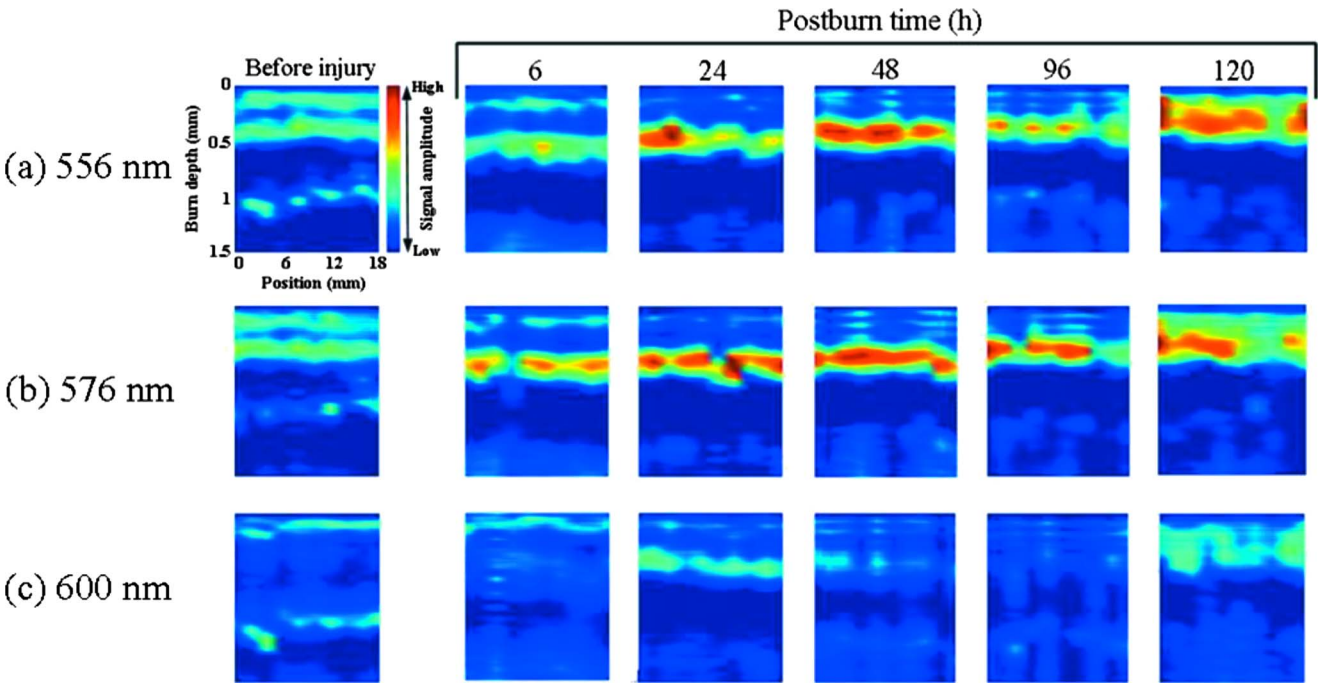

Fig. 7 PA tomograms before and after making a deep dermal burn in a rat at (a) 556, (b) 576, and (c) 600 nm. The region of high PA signal amplitudes is shown in red. (Color online only.)

making a deep dermal burn. The PA tomograms at 556, and 576 nm showed a tendency similar to that at 532 nm (Fig. 3). The tomogram at 600 nm before injury showed two signal layers with low to medium amplitudes in the depth ranges of 0.1–0.2 and 0.7–0.8 mm. The latter signal layer had disappeared at 6 h, but a signal layer with medium amplitude appeared in the depth range of 0.4–0.5 mm at 24 h; the signal amplitude in this layer gradually decreased with the elapse of time, but a broad signal layer with low to medium amplitudes was observed in a shallower region, 0.2–0.3 mm, at 120 h.

Figure 8 shows typical time courses of PA signal amplitudes at all wavelengths for a rat, where amplitudes are normalized by those at the earliest postburn time, 1.5 h, and each plot represents an averaged value for 10 measurement points in the rat. At 532, 556, and 576 nm, signal amplitudes generally increased for up to 48 h postburn time, and thereafter, they gradually decreased for up to 96 h postburn time. At 600 nm, signal amplitude decreased from 24 to 48 h, and there was a significant difference in signal amplitude between 600 nm and any other wavelengths in this particular time domain ($P<0.05$). Figure 9 shows the time courses of PA signal amplitudes for all rats used in this study ($n=5-8$). A tendency similar to that in Fig. 8 was observed. There was a significant difference between signal amplitude at 600 nm and signal amplitudes at any other wavelengths from 24 to 48 h ($P<0.01$). At all wavelengths, the amplitudes decreased from 72 to 96 h and increased again from 96 to 120 h postburn time.

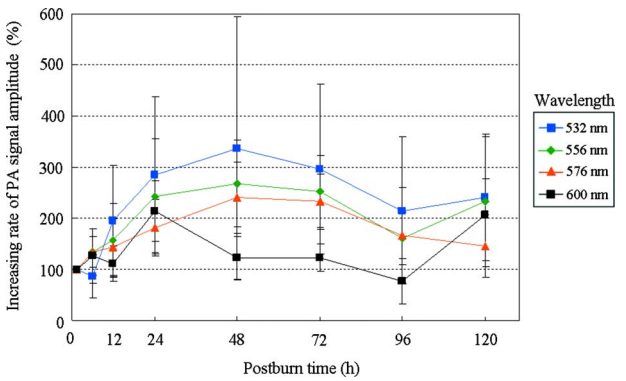

Fig. 8 Typical time courses of PA signal amplitudes at all wavelengths for a rat, where amplitudes are normalized by those at the earliest postburn time, 1.5 h, and each plot represents an averaged value for 10 measurement points in the rat. Values are expressed as means ± standard error.

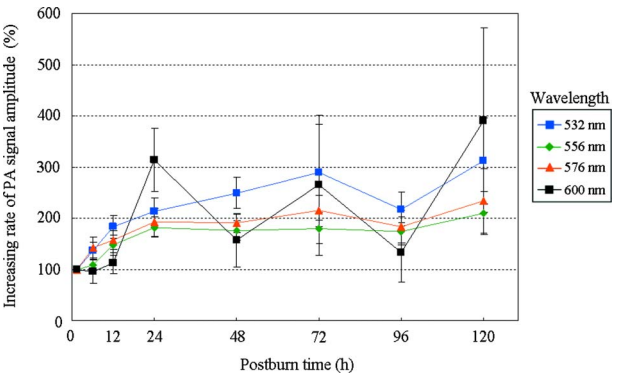

Fig. 9 Time courses of PA signal amplitudes at all wavelengths for all rats used in this study ($n=5-8$), where amplitudes are normalized by those at 1.5 h postburn time. Values are expressed as means ± standard error.

4 Discussion

In the present study, we attempted to observe the recovery of blood perfusion and change in hemodynamics in deep dermal burns in rats by PA measurements for monitoring the healing process of the wounds. In the PA tomogram at the postburn time of 1.5 h (Fig. 3), two signal layers were observed at depths of about 0.2 mm and 0.6 mm; the shallower layer disappeared for up to 24 h postburn time, while the signal amplitudes for the deeper layer became larger for up to 72 h postburn time. In tissues that are thermally injured, blood flow is gradually interrupted due to the occlusion of arteriola, alteration of microvascular endothelium and formation of clots.[22] Thus, the disappearance of the shallower signal layer is attributable to the vascular occlusion. The deeper signal layer is thought to originate from the blood in healthy tissue under the injured tissue layer; the region above this layer indicates the zone of stasis and hence injured tissue layer. The reason for the site-dependent variation of PA signals in spite of uniform heating being used to make burns is thought to be inhomogeneous skin thickness and vascular distribution and, as a result, the healing process might also be site dependent.

After 6 h postburn time, the depth of the PA signal giving the highest amplitude at each position gradually shifted to a shallower region, and it was ~0.35 mm at a postburn time of 120 h (Fig. 3). The results of histological analysis of the wounds showed increased density and extended distribution of neovascularities with the elapse of time; at 120 h, high-density CD31-positive cells (i.e., neovascularities) were observed in the depth range of 0.2–1.2 mm (Figs. 5 and 6). These findings suggest that the shift of PA signals to the shallower region reflects recovery of blood perfusion in the injured tissues. It should be noted, however, that PA signal peaks were observed in a region deeper than the depths at which neovascularities observed. This is presumably due to the fact that blood vessels are formed after repeated divisions and proliferation of vascular endothelial cells, which are stained with CD31/PECAM-1 antibody, and they should be surrounded by pericytes. Thus, CD31-positive cells are thought to appear earlier than the restart of blood perfusion and hence the observation of blood-originated PA signals.

As described above, severe burns show phase-dependent unique abnormalities in systemic circulation dynamics, which also affect the local hemodynamics in skin. The wavelength-dependent changes in time courses of signal amplitudes (Figs. 8 and 9) are thought to reflect change in local hemodynamics in the wounds. For up to 24 h postburn time, signal amplitude increased at all wavelengths. We speculate that this is associated with dilation of blood vessels within healthy tissue under the injured tissue layer[23,24] and increase in the concentration of red blood cells [i.e., hematocrit (HCT)] due to development of edema. Edema is a common symptom caused by severe burns, in which plasma components leak out of the blood vessels due to increased vascular permeability, resulting in increased HCT. For extensive burns, edema develops not only in the wounds and their peripheries, but also in the whole body due to damage to blood vessels in many organs, resulting in systemic condensation of blood and hence increase in HCT.[4] Actually, we observed evident edema in this time period. During the postburn time of 24–48 h, the signal amplitudes at 532, 556, and 576 nm continued to increase, while the signal amplitude at 600 nm decreased. Passing through the shock phase, hemodynamics shifts to that in the hyperdynamic state; in this state, oxygen consumption (HHb) associated with hypermetabolism is increased and cardiac output (HbO_2) is abnormally increased to maintain the increased oxygen consumption. However, oxygen delivery to peripheral tissues is inadequate because oxygen intake is blocked by edema. Therefore, the level of HHb is decreased due to the increase in the HbO_2 within the wounds. Thus, the hyperdynamic state is an indicator of leaving the shock phase. The wavelength-dependent change in amplitude we observed is likely to reflect the change from a shock phase to the phase of a hyperdynamic state in the body with severe burns.

After a postburn time of 72 h, signal amplitudes at all wavelengths showed a similar tendency; they decreased from 72-to 96-h postburn time and increased again from 96-to 120-h postburn time. After 72-h postburn time, we found that edema was decreased and the color of the wound surface was becoming reddish. Thus, the increased signal amplitudes observed during the postburn period of 72–96 h can be interpreted by being due to normalization of increased vascular permeability, by which blood vessels would be refilled with massive fluid in the tissue, resulting in decrease in HCT. After 96 postburn time, signal amplitudes increased again probably due to recovery of peripheral circulation disorder in this time range.

It should be noted that the levels of light scattering in the tissue might also change during the healing of the wound. We previously reported that by using the same piezoelectric film as that used for PA measurement, the light-scattering level can also be monitored, based on pyroelectricity of the film; for example, increase in light scattering causes an increase in intensity of the pyroelectric signal due to transient heating of the sensor.[25] In this study, we observed a dramatic difference between pyroelectric signals before and after making burns, but the postburn change was relatively small, suggesting that scattering change due to the wound healing appears later (i.e., after 120 h postburn time).

For clinical application of PA diagnosis of burns, the need for ultrasound gel is disadvantageous in terms of sterility, influence on ointment used for treatment, patient comfort, etc. Sterilized water can be used in some cases as an alternative ultrasound couplant. In addition, in cases in which a thin, transparent wound dressing, such as hydrocolloid and polyurethane film, is used,[26,27] PA measurement may be possible over the dressing with ultrasound gel; recently, these dressings have been widely used for managing severe burn injuries.

In conclusion, our multiwavelength PA measurement provided two data sets that are considered to reflect the wound-healing process of burns: (*i*) time-dependent change in the signal peak depth due to recovery of blood perfusion and (*ii*) time- and wavelength-dependent changes in the signal amplitudes probably due to the hyperdynamic state. Although four wavelengths were used in this study, only the signal at 600 nm showed behavior that seems to be associated with a hyperdynamic state, and recovery of blood perfusion can be monitored at this wavelength. We can therefore monitor the wound-healing process by using only 600 nm or by using 600 nm plus 1 of the other wavelengths to serve as a reference signal of blood volume or HbO_2. To confirm the validity

of this technique for monitoring peripheral hemodynamics, we plan to directly measure the cardiac output, blood pressure, HCT, and amount of urea and to compare PA signals to the results of these measurements. We will also investigate the feasibility of quantitative evaluation of oxygenation level and hemoglobin concentration in the blood based on PA measurement; quantitative information on oxygen delivery to the wound is very important to diagnose the state of the wound.[28]

Because burn thickness is less than ~1 mm in rat models, we investigated the applicability of our method to diagnosis of deeper burns with a mimic deep burn model; we put excised burned skin(s) on the wound of a rat burn model and attempted to measure the blood-originating PA signal. The results of the experiment showed that the PA signal originating from blood under injured tissue layers as thick as >3 mm can be detected by increasing the laser pulse energy (data not shown). As the next step, we plan to perform multiwavelength PA measurement for a porcine burn model, which has a closer anatomical resemblance to human skin. It has been revealed recently that various types of genes and cytokines are involved in the healing process of wounds. Muiltiwavelength PA measurement can also be a powerful tool to investigate the usefulness of gene therapy and regeneration medicine for severe traumatic injuries (e.g., gene transfer of a growth factor to injured tissues or grafts for promoting angiogenesis).[29–32]

Acknowledgments

The authors acknowledge financial support from the Cosmetology research foundation and the Nakatomi Foundation.

References

1. T. T. Nguyen, D. A. Gilpin, N. A. Meyer, and D. N. Hemdon, "Current treatment of severely burned patients," *Ann. Surg.* **223**, 14–25 (1996).
2. W. R. Schiller and R. C. Bay, "Hemodynamic and oxygen transport monitoring management of burns," *New Horiz* **4**, 475–482 (1996).
3. K. L. Mattox, *Trauma*, McGraw-Hill, New York (2000).
4. R. H. Demling, *Burn Trauma*, Thieme Medical Publishers, New York (1989).
5. A. B. Wysocki, "Wound management," *Int. J. Dermatol.* **35**, 82–91 (1996).
6. F. W. H. Kloppenberg, G. M. Beerthuizen, and H. J. ten Duis, "Perfusion of burn wounds assessed by laser Dopper Imaging is related to burn depth and healing time," *Burns* **27**, 539–363 (2001).
7. B. S. Atiyeh, S. W. Gunn, and S. N. Hayek, "State of the art in burn treatment," *World J. Surg.* **29**, 131–148 (2005).
8. M. Green, G. A. Holloway, and D. M. Heimbach, "Laser Doppler monitoring of microcirculatory changes in acute burn wounds," *J. Burn Care Rehabil.* **9**, 57–62 (1988).
9. M. I. Liddington and P. G. Shakespeare, "Timing of the thermographic assessment of burns," *Burns* **22**, 26–28 (1996).
10. L. P. Kamoloz, H. Andel, and W. Haslik, "Indocyanine green video angiographies help to identify burns requiring operation," *Burns* **29**, 785–791 (2003).
11. A. T. Yeh, B. Kao, W. G. Jung, Z. Chen, J. S. Nelson, and B. J. Tromberg, "Imaging wound healing using optical coherence tomography and multiphoton microscopy in an *in vitro* skin-equivalent tissue model," *J. Biomed. Opt.* **9**, 014017 (2004).
12. M. J. Cobb, Y. Chen, R. A. Underwood, M. L. Usui, J. Olerud, and X. Li, "Noninvasive assessment of cutaneous wound healing using ultrahight-resolution optical coherence tomography," *J. Biomed. Opt.* **11**, 064002 (2006).
13. S. Sato, M. Yamazaki, D. Saitoh, H. Tsuda, Y. Okada, M. Obara, and H. Ashida, "Photoacoustic diagnosis of burns in rats," *J. Trauma: Inj., Infect., Crit. Care* **59**, 1450–1455 (2005).
14. M. Yamazaki, S. Sato, D. Saitoh, Y. Okada, H. Ashida, and M. Obara, "Measurement of burn depths in rats using multiwavelength photoacoustic depth profiling," *J. Biomed. Opt.* **10**, 064011 (2005).
15. H. F. Zhang, K. Maslov, G. Stoica, and L. V. Wang, "Imaging acute thermal burns by photoacoustic microscopy," *J. Biomed. Opt.* **11**, 054033 (2006).
16. X. Wang, Y. Pang, G. Ku, G. Stoica, and L. V. Wang, "Non-invasive imaging of hemoglobin concentration and oxygenation in the rat brain using high-resolution photoacoustic tomography," *J. Biomed. Opt.* **11**, 024015 (2006).
17. J. Laufer, D. Delpy, C. Elwell, and P. Beard, "Quantitative spatially resolved measurement of tissue chromophore concentrations using photoacoustic spectroscopy: Application to the measurement of blood oxygenation and hemoglobin concentration," *Phys. Med. Biol.* **52**, 141–168 (2007).
18. R. O. Esenaliev, I. V. Larina, K. V. Larin, D. J. Deyo, M. Motamedi, and D. S. Prough, "Optoacoustic technique for noninvasive monitoring of blood oxygenation: a feasibility study," *Appl. Opt.* **41**, 4722–4731 (2002).
19. A. Tandara and T. Mustoe, "Oxygen in wound healing—more than a nutrient," *World J. Surg.* **28**, 294–300 (2004).
20. H. L. Walker and A. D. Mason, "A standard animal model," *J. Trauma* **8**, 1049–1051 (1968).
21. R. A. Kruger, W. L. Kiser, D. R. Reinecke, G. A. Kruger, and K. D. Miller, "Thermoacoustic optical molecular imaging of small animals," *Mol. Imaging* **2**, 113–123 (2003).
22. K. N. Ham and J. V. Hurley, "An electron-microscope study of the vascular response to mild thermal injury in the rat," *J. Pathol. Bacteriol.* **95**, 175–183 (1968).
23. B. E. Zawacki, "Reversal of capillary stasis and prevention of necrosis in burns," *Ann. Surg.*, **180**, 98–104 (1974).
24. B.-M. Kim, S. L. Jacques, S. Rastegar, S. Thomsen, and M. Motamedi, "Benign prostatic hyperplasia," *IEEE J. Sel. Top. Quantum Electron.*, **2**, 922–933 (1996).
25. M. Yamazaki, S. Sato, D. Saitoh, Y. Okada, H. Ashida, and M. Obara, "*In vivo* scattering measurement of biological tissue by the use of a pyroelectric polymer transducer," *Appl. Opt.* **44**, 1591–1594 (2005).
26. J. W. Beam, "Management of superficial to partial-thickness wounds," *J. Athletic Training* **42**, 422–424 (2007).
27. M. H. E. Hermans, "A general overview of burn care," *Int Wound J.* **2**, 206–220 (2005).
28. B. Venkatesh, R. Meacher, M. J. Mullar, T. J. Morgan, and J. Fraser, "Monitoring tissue oxygenation during resuscitation of major burns," *J. Trauma: Inj., Infect., Crit. Care* **50**, 485–494 (2001).
29. R. Gurunluglu, R. Meirer, G. M. Huemer, B. Yilmaz, and H. Pizakatzer, "Gene therapy with adenovirus-mediated VEGF enhances skin flap prefabrication," *Microsurgery* **25**, 433–441 (2005).
30. P. Lubiatowski, C. K. Goldman, R. Gurunluoglu, K. Carnevale, and M. Siemionow, "Enhancement of epigastric skin flap survival by adenovirus-mediated VEGF gene therapy," *Plast. Reconstr. Surg.* **109**, 1986–1993 (2002).
31. P. Y. Liu, K. Liu, X. T. Wang, E. Badiavas, K. M. Rieger-Christ, J. B. Tang, and I. C. Summerhayes, "Efficacy of combination gene therapy with multiple growth factor cDNAs to enhance skin flap survival in a rat model," *DNA Cell Biol.* **24**, 751–757 (2005).
32. M. Terakawa, S. Sato, D. Saitoh, H. Tsuda, H. Ashida, H. Okano, and M. Obara, "Enhanced angiogenesis in grafted skins by laser-induced stress wave-assisted gene transfer of hepatocyte growth factor," *J. Biomed. Opt.* **12**, 034031 (2007).